Ocean Engineering 53 (2012) 48–59

Contents lists available at SciVerse ScienceDirect

Ocean Engineering

journal homepage: www.elsevier.com/locate/oceaneng

# Three-dimensional consolidation of a porous unsaturated seabed under rubble mound breakwater

D.-S. Jeng [a,b,*], J.H. Ye [b]

[a] Center for Marine Geotechnical Engineering, Department of Civil Engineering, Shanghai Jiao Tong University, Shanghai 200240, China
[b] Division of Civil Engineering, University of Dundee, Dundee, DD1 4HN, UK

ARTICLE INFO

*Article history:*
Received 3 February 2012
Accepted 2 June 2012
Editor-in-Chief: A.I. Incecik
Available online 11 July 2012

*Keywords:*
Consolidation
Biot's theory
Rubble mound breakwater
Seabed
Poro-elasticity
Hydrostatic pressure

ABSTRACT

The consolidation status of a seabed under marine structures and hydrostatic pressure is the basis for the evaluation of the liquefaction and dynamic shear failure of seabed foundation under ocean wave loading. However, only a few investigations have been conducted for the seabed consolidation under hydrostatic pressure and marine structures. Furthermore, most previous numerical models for the Biot's consolidation theory are limited to two-dimensional cases. In this study, based on Biot's dynamic poro-elastic theory ("$u-p$" approximation), a three-dimensional FEM seabed model is adopted to investigate the consolidation of seabed under a rubble mound breakwater and hydrostatic pressure. Numerical results show that the rubble mound breakwater significantly affect the stress/displacement fields in the seabed foundation. Based on the parametric study, it can be concluded: (1) Young's modulus of a seabed significantly affects the settlement of breakwater; and (2) the magnitude of the shear stress concentrates in the zones beneath the toes of breakwater.



## 1. Introduction

More than two-thirds of the world's population is concentrated in the coastal zones, where has been the center of economic development. In coastal zones, the coastal structures, such as rubble mound breakwater, have been commonly used for the protection of the coastline from damage and erosion. It has been reported in the literature that numerous breakwaters were vulnerable to the liquefaction and the shear failure of seabed foundation (Chung et al., 2006; Franco, 1994; Lundgren et al., 1989). An inappropriate design of the breakwater would result in the collapse of breakwaters.

It has been well known that the seabed generally has experienced the consolidation process under the hydrostatic pressure and the self-gravity in the geological history. In engineering practice, self-weight of a breakwater is initially transferred to the pore water in a seabed foundation, resulting in the generation of excess pore pressure and pressure gradient. After a while, the pore water permeates driven by the pressure gradient through the void between soil particles, promoting the pore pressure dissipate gradually. In this process, the gravity of breakwater is gradually transferred from the pore water to the soil particles; and the breakwater subsides correspondingly. Finally, the seabed foundation reaches an equilibrium consolidation status. This consolidation status should be the initial condition for evaluation of the dynamic response of seabed foundation and breakwater under dynamic loading. However, most previous investigations have not considered this consolidation status of seabed foundation under hydrostatic pressure and breakwater as the initial condition by assuming that all initial values, including displacements, velocity, stresses and pore pressures, being zeros (Mase et al., 1994; Mizutani et al., 1998; Mostafa et al., 1999; Jeng et al., 2001; Wang et al., 2007, 2004). This assumption would make the predictions of liquefaction and dynamic shear failure of seabed foundation to be doubtable. Therefore, the determination of the initial consolidation status of seabed foundation under hydrostatic pressure and breakwater is an essential step in evaluation of the stability of marine structures. Recently, Ulker et al. (2010) may be the first considered the effects of pre-consolidation in the assessment of the standing wave-induced liquefaction in front of a caisson breakwater, but it was limited to two-dimensional cases.

The first researcher investigating the consolidation problem was Terzaghi (1925) who proposed an analytical solution of 1D soil volume. Later, Biot (1941) further proposed a three-dimensional general theory for the soil consolidation, which has been widely adopted to investigate the phenomenon of the flow and deformation process in porous media. In general, exact solutions of consolidation problems of soil are difficult to obtain due to the complex boundary conditions. Most numerical studies for the Biot's consolidation equation focused on the numerical technique of solving the Biot's consolidation equation, and the

* Corresponding author. Tel.: +44 1382386141; fax: +44 1382384816.
*E-mail addresses:* d.jeng@dundee.ac.uk, jengd2@asme.org (D.-S. Jeng).

0029-8018/$ - see front matter © 2012 Elsevier Ltd. All rights reserved.
http://dx.doi.org/10.1016/j.oceaneng.2012.06.004

corresponding convergence and stability (Booker, 1973; Cavalcanti and Telles, 2003; Ferronato et al., 2010; Hua, 2011; Korsawe et al., 2006; Miga et al., 1998; Sloan and Abbo, 1999; Wang et al., 2009). Furthermore, most previous numerical models for the consolidation of soil have been limited to two-dimension (Kelln et al., 2009; Yin and Zhu, 1999). However, two-dimensional models are insufficient to determine the consolidation status of the seabed foundation beneath a rubble mound breakwater, which requires a three-dimensional model. Therefore, in this study, a three-dimensional FEM model for Biot's consolidation theory is adopted to examine the consolidation of a rubble mound breakwater under self-weight of the structure and hydrostatic water pressures in marine environments.

## 2. Boundary value problem

### 2.1. Governing equation

It has been well known that the seabed is porous medium consisting of the soil particles, pore water and trapped air. The Biot's poro-elastic theory has been commonly used to describe the mechanical behaviour of porous medium. In this paper, the consolidation of three-dimensional seabed under rubble mound breakwater, as depicted in Fig. 1 is studied. The seabed is treated as a poro-elastic, isotropic and homogeneous porous medium. The Biot's dynamic poro-elastic theory ("$u-p$" approximation Zienkiewicz et al., 1980) is used as the governing equation for porous seabed and the rubble mound breakwater. The relative displacements of pore water to the soil particles are ignored, but the acceleration of the soil particles is included.

$$\frac{\partial \sigma'_x}{\partial x}+\frac{\partial \tau_{xy}}{\partial y}+\frac{\partial \tau_{xz}}{\partial z}=-\frac{\partial p_s}{\partial x}+\rho\frac{\partial^2 u_s}{\partial t^2}, \tag{1}$$

$$\frac{\partial \tau_{xy}}{\partial x}+\frac{\partial \sigma'_y}{\partial y}+\frac{\partial \tau_{yz}}{\partial z}=-\frac{\partial p_s}{\partial y}+\rho\frac{\partial^2 v_s}{\partial t^2}, \tag{2}$$

$$\frac{\partial \tau_{xz}}{\partial x}+\frac{\partial \tau_{yz}}{\partial y}+\frac{\partial \sigma'_z}{\partial z}+\rho g=-\frac{\partial p_s}{\partial z}+\rho\frac{\partial^2 w_s}{\partial t^2}, \tag{3}$$

$$k\nabla^2 p_s-\gamma_w n\beta\frac{\partial p_s}{\partial t}+k\rho_f\frac{\partial^2 \epsilon}{\partial t^2}=\gamma_w\frac{\partial \epsilon}{\partial t}, \tag{4}$$

where $(u_s,v_s,w_s)$ are soil displacements in the $x$, $y$, $z$ directions, respectively; $n$ is soil porosity; $\sigma'_x$, $\sigma'_y$ and $\sigma'_z$ are effective normal stresses in the horizontal and vertical directions, respectively; $\tau_{xy}$, $\tau_{xz}$ and $\tau_{yz}$ are shear stresses; $p_s$ is the pore pressure in seabed; $\rho=\rho_f n+\rho_s(1-n)$ is the average density of porous seabed; $\rho_f$ = the fluid density; $\rho_s$ = solid density; $k$=the Darcy's permeability (the seabed in this study is treated as isotropic); $g$ is the gravitational acceleration and $\epsilon$ denotes the volumetric strain.

In Eq. (4), the compressibility of pore fluid ($\beta$) and the volume strain ($\epsilon$) are defined as

$$\beta=\left(\frac{1}{K_f}+\frac{1-S_r}{p_{w0}}\right),\quad \text{and}\quad \epsilon=\frac{\partial u_s}{\partial x}+\frac{\partial v_s}{\partial y}+\frac{\partial w_s}{\partial z}, \tag{5}$$

where $S_r$ is the degree of saturation of seabed, $p_{w0}$ is the absolute static pressure and $K_f$ is the bulk modulus of pore water.

### 2.2. Boundary conditions

The computational domain shown in Fig. 1 is a large scale seabed-breakwater model. The size of seabed is 370 m × 370 m × 30 m (Length × Width × Thickness) and a rubble mound breakwater (Length=220 m, Bottom width=53 m, Height=16 m, Slope gradient=2:3) is built on the seabed. The boundary conditions applied to this computational domain are outlined here.

First, the bottom of the seabed is considered as rigid and impermeable

$$u_s=v_s=w_s=0\quad\text{and}\quad\frac{\partial p_s}{\partial z}=0. \tag{6}$$

Second, the displacement $v_s$ at the front and back boundary generally are apparently small. Therefore, the front and back boundary $y=0$ m and $y=370$ m are both fixed at $y$-direction

$$v_s=0\quad\text{at } y=0\text{ m and } y=370\text{ m}. \tag{7}$$

Finally, the hydrostatic pressure is applied on the surface of seabed and the outer surface of rubble mound breakwater. However, the interface between the rubble mound and seabed is not applied by the hydrostatic pressure because that it is an inner boundary of computational domain. All hydrostatic pressure is perpendicular with the surfaces, as shown in Fig. 2.

In this study, a three-dimensional finite element model (FEM) is developed to solve the above boundary value problem. The main focus of this model is to examine the effects of rubble mound breakwaters on the consolidation process of the seabed foundation before dynamic loading is applied. As mentioned previously, the existing model developed by the first author's group, PORO-WSSI II (Porous model for Wave-Seabed-Structure

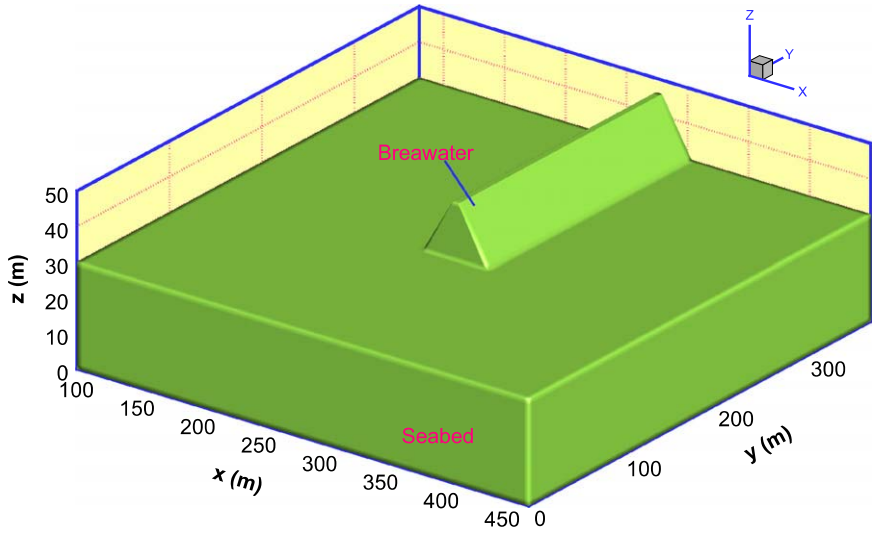


**Fig. 1.** The computational domain of the three-dimensional seabed and breakwater.

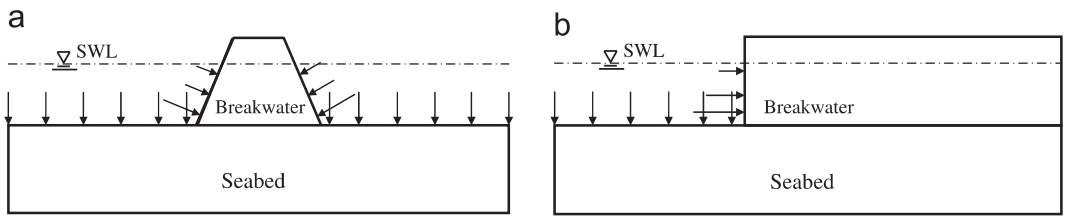


**Fig. 2.** The schematic map of hydrostatic pressure acting on the rubble mound breakwater and seabed. (a) Section $x=180$ m and (b) Section $y=276.5$ m.

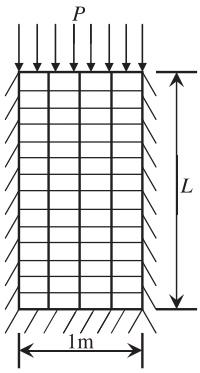


**Fig. 3.** One-dimensional soil volume used in Terzaghi's consolidation theory.

**Table 1**
Parameters used in the verification case with Terzaghi model.

| | |
|---|---|
| Young's modulus | $10^8$ N/m$^2$ |
| Poisson's ratio | 0.25 |
| Permeability | $1.0\times10^{-5}$ m/s |
| Porosity | 0.375 |
| $L$ | 20 m |
| $P$ | 10 kPa |
| $\beta$ | $4.4\times10^{-10}$ m$^2$/N |
| $\lambda$ | 40 MPa |
| $\mu$ | 40 MPa |
| $\alpha$ | 1.0 |

Interaction, Version II) (Zhang et al., 2011), has not considered the pre-consolidation as well as other existing models reported in the literature. The proposed model will form part of PORO-WSSI III (Version 3 for three-dimensional cases), which was first developed by Jeng and Ou (2010) with our pre-consolidation. Taking the final consolidation status obtained from this study as the initial condition, the dynamic response of seabed foundation and rubble mound breakwater is then calculated. A new loading system developed can deal with various types of loading on arbitrary planes at arbitrary directions, which has been limited to a specific loading in Jeng and Ou (2010).

## 3. Verification of three-dimensional FEM soil model—Terzaghi's consolidation theory

In this section, the consolidation modulus of this developed three-dimensional FEM soil model is validated by the one-dimensional Terzaghi's consolidation theory. A one-dimensional poro-elastic, isotropic, homogeneous and fully saturated soil volume with height $L$ is applied by a constant stress $P$ (the other two dimensions are both 1 m, see Fig. 3). The one-dimensional soil volume is consolidated under the constant stress. The drainage is only allowed through the surface where the constant stress is applied. The bottom of soil volume is fixed and impermeable. As shown in Fig. 3, the $z$-axis is positive upward, and the surface on which the stress applying is taken as $z=0$). Wang (2000) proposed an analytical solution for the pore pressure and displacement variation in consolidation process,

$$p_s(z,t)=\frac{4}{\pi}p_{s0}\sum_{m=0}^{m=\infty}\frac{1}{2m+1}\exp\frac{-(2m+1)^2\pi^2c_vt}{4L^2}\sin\frac{-(2m+1)\pi z}{2L}, \tag{8}$$

$$w_s(z,t)=c_mp_{s0}\left\{(L+z)-\frac{8L}{\pi^2}\sum_{m=0}^{m=\infty}\frac{1}{(2m+1)^2}\exp\frac{-(2m+1)^2\pi^2c_vt}{4L^2}\cos\frac{(2m+1)\pi z}{2L}\right\}+w_{s0}, \tag{9}$$

where $p_{s0}$ and $w_{s0}$ is the instantaneous pore pressure and displacement in soil volume induced by the constant stress $P$ at time $t=0$, expressed as

$$p_{s0}=\frac{\alpha MP}{K_u+4\mu/3}\quad\text{and}\quad w_{s0}=\frac{(L+z)P}{K_u+4\mu/3}, \tag{10}$$

in which $M=(n\beta+(\alpha-n)K_s)^{-1}$ is the Biot modulus, $K_s$ is the compressibility of soil skeleton, $n$ is the porosity. $K_u=\lambda+2\mu/3+\alpha^2M$ is the undrained bulk modulus. $c_m=(\lambda+2\mu)^{-1}$ is the vertical unaxial compressibility. $c_v=k/(\rho g(M^{-1}-\alpha^2c_m))$ is the consolidation coefficient. The parameters used in this verification case is listed in Table 1.

Fig. 4(a) and (b) illustrate the distributions of pore pressures and the displacements in the soil column at various time, while Fig. 4(c) presents the historical curve of the settlement versus time. Numerical results from both the present numerical model and the previous analytical solution (Wang, 2000) are included in the figures. As shown in the numerical comparisons, good agreements between two models are observed.

## 4. Results and discussions

In this study, three-dimensional iso-parametric brick elements with 27 nodes are used to discrete the computational domain, which is the third-order approximation in finite element modelling, deserving highly accurate results. The properties of a sandy seabed and rubble mound breakwater used in numerical examples are listed in Table 2.

It has been well known that the consolidation of any type foundation, including the seabed foundation does not complete instantaneously because that the structure gravity induced excess pore pressure in seabed foundation dissipates gradually. To reach the status of completed consolidation, it requires a certain time, which varies from years (for clays with extremely low permeability) to hours (for coarse sand). This also depends on the soil permeability, length of drainage path, and compressibility of soil, etc. In this study, to ensure the sandy seabed consolidate sufficiently in the computational time, the full consolidation time for a sandy seabed under hydrostatic pressure is estimated by the 1-D consolidation theory. The time for completing 90% of the

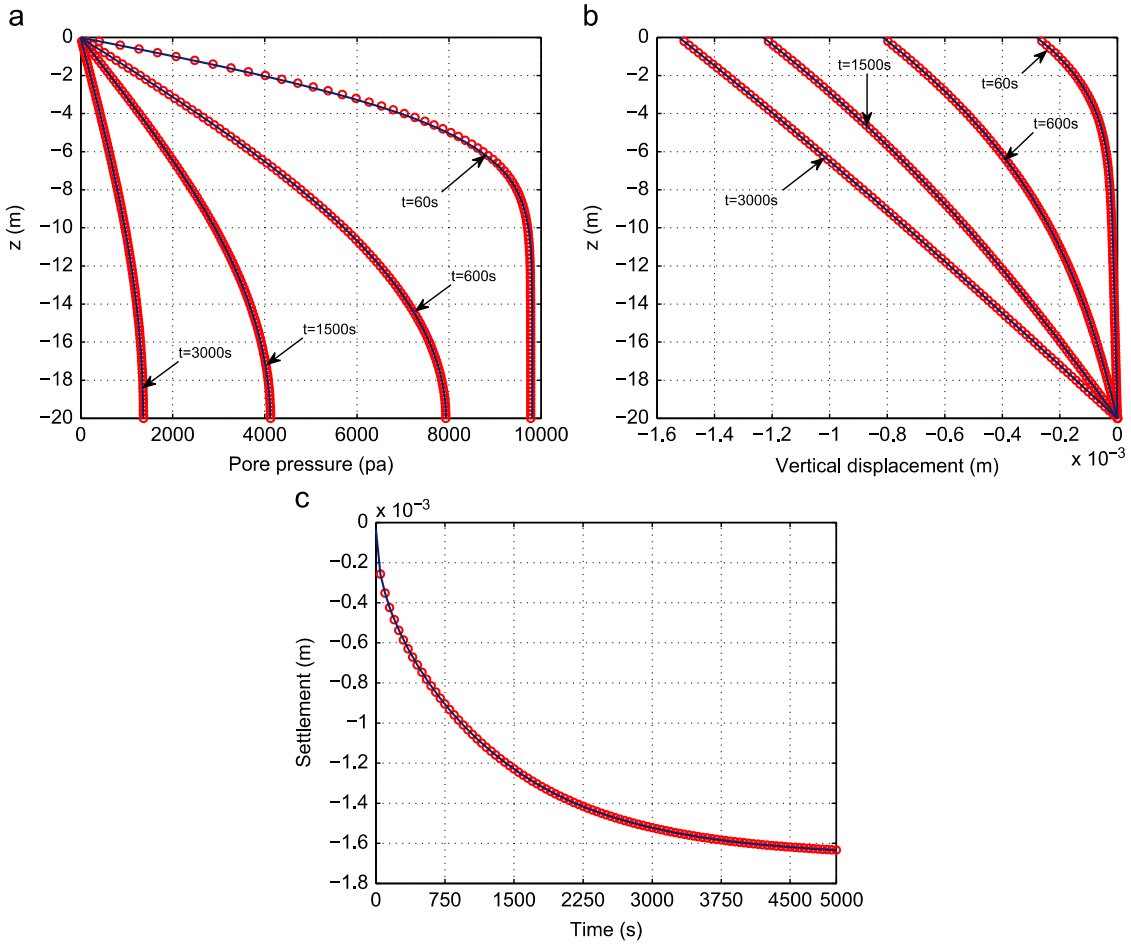


**Fig. 4.** The distributions of (a) pore pressure and (b) vertical displacement along and (c) settlement of the 1-D soil volume under a constant compressive stress $P=10$ kPa. Notation: solid lines=the present model; symbols=1-D model.

**Table 2**
Properties of sandy seabed and the rubble mound breakwater adopted in calculation.

| Object | $G$ (N/m$^2$) | $\mu$ | $S_r$ (%) | $k$ (m/s) | $n$ | Special gravity |
|---|---|---|---|---|---|---|
| Seabed | $6.0\times10^7$ | 0.3333 | 98 | $1.0\times10^{-4}$ | 0.3 | 2650 |
| Breakwater | $1.0\times10^9$ | 0.25 | 100 | $2.0\times10^{-1}$ | 0.35 | 2650 |

consolidation $t_{90}$ is formulated as (Wang, 2000)

$$t_{90}=T_v\frac{H_d^2}{c_v}\quad\text{where } c_v=\frac{2G(1-\mu)k}{\gamma_w(1-2\mu)}, \tag{11}$$

where $T_v$ is the vertical consolidation time factor, it is 0.848 corresponding to 90% of the consolidation; the consolidation coefficient ($c_v$) depends on the shear modulus of soil, and Poisson's ratio; $H_d$ is the drainage distance, which is taken as the thickness of the porous seabed here.

With the parameters of seabed given in Table 2, the time $t_{90}$ can be determined. In this study, the computation time is chosen as 6000 s, which is sufficient for full consolidation of the sandy seabed under hydrostatic pressure and rubble mound breakwater. Fig. 5 illustrates the historical curve of the pore pressure and vertical effective stress at the point, $(x, y, z)=(276.5, 180, 25.2)$ m, where it is under the rubble mound breakwater. It is found that the pore pressure in seabed under the rubble mound breakwater is fully dissipated. At the time $t=6000$ s, the seabed basically completes the consolidation process under hydrostatic pressure and rubble mound breakwater.

### 4.1. *Effective stresses and pore pressures*

Fig. 6 illustrates the distribution of the pore pressure ($p_s$), vertical effective normal stress ($\sigma'_z$) and shear stresses ($\tau_{xy}$, $\tau_{yz}$, $\tau_{xz}$) in a seabed at two typical sections $y=98.7$ and $x=167.5$ m, which can be considered far from the rubble mound breakwater. As shown in the figure, it is found that the pattern of distributions of $p_s$ and $\sigma'_z$ is layered. In fact, a similar pattern has been found for $\sigma'_x$ and $\sigma'_y$ (graphs not shown). This implies that the effects of the rubble mound breakwater on the pore pressure ($p_s$), and effective normal stresses ($\sigma'_x$, $\sigma'_y$ and $\sigma'_z$) disappear in the region far away from the breakwater. However, the effects of breakwater on the shear stresses $\tau_{xy}$, $\tau_{yz}$, $\tau_{xz}$ are visible at these two sections (Fig. 6). Certainly, this effect will also decrease gradually with the distance to the breakwater. After numerical study, the influenced ranges of the breakwaters on shear stresses approximately are: $x=150$–400 m, $y=0$–300 m for $\tau_{xy}$, $\tau_{yz}$, and $x=150$–420 m, $y=50$–370 m for $\tau_{xz}$.

Figs. 7 and 8 show the distributions of pore pressure, effective stresses and shear stresses in a seabed at sections $y=181.1$ m and $x=277$ m. As shown in the figures, the effect of rubble mound breakwater on the stress field can be observed more clearly. Since the excess pore pressure induced by the breakwater has dissipated sufficiently, the seabed has consolidated sufficiently. The pattern of distributions of the pore pressure is layered in a seabed.

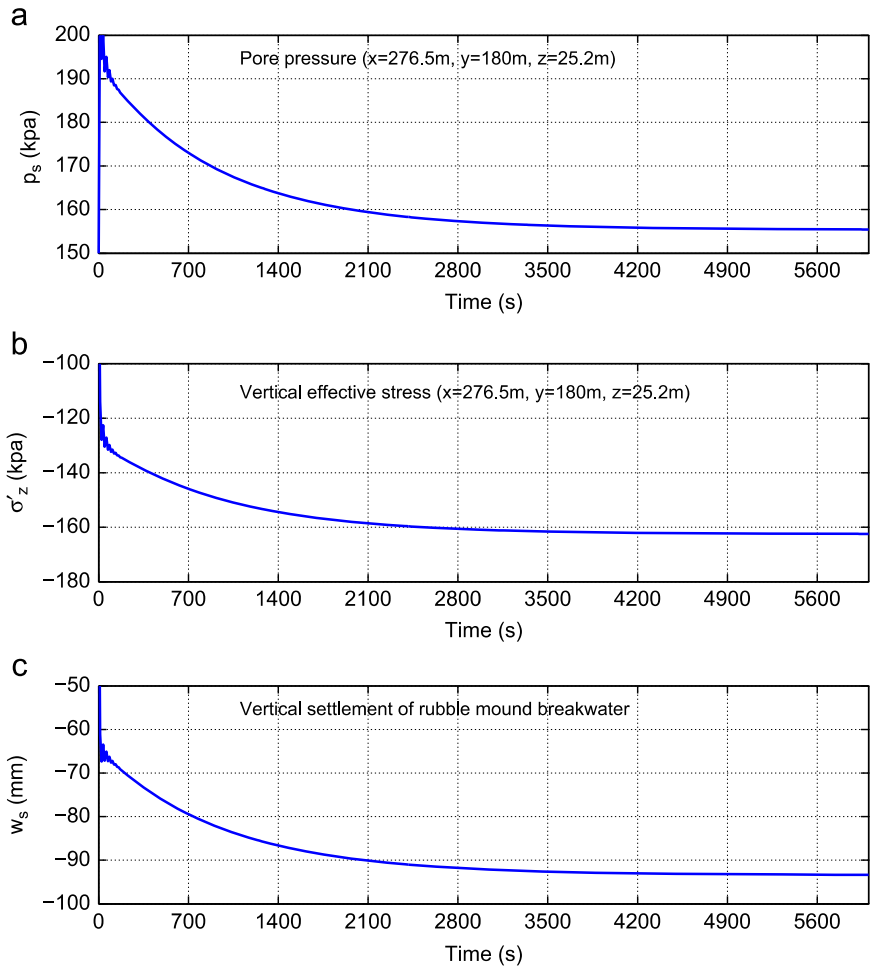


**Fig. 5.** The historic curves of (a) pore pressure $p_s$ and (b) effective normal stress $\sigma'_z$ at the point $(x,y,z)=(276.5, 180, 25.2)$ m, and (c) the vertical settlement of rubble mound breakwater in the process of consolidation.

Regarding distributions of $\sigma'_x$, $\sigma'_y$ and $\sigma'_z$, it is found that the effect of breakwater on the $\sigma'_x$, $\sigma'_y$ and $\sigma'_z$ is significant. The magnitude of $\sigma'_x$, $\sigma'_y$ and $\sigma'_z$ increase greatly in seabed under the rubble mound breakwater. In the region far from the breakwater, the effect of breakwater on the $\sigma'_x$, $\sigma'_y$ and $\sigma'_z$ basically disappear as expected. It is interesting to note that there is a tensile stress concentration zone between the breakwater and the seabed for $\sigma'_x$ and $\sigma'_y$. This is because that the seabed moves toward two lateral sides and toward the $y$-direction under the gravity of breakwater. However, because the breakwater is much stiffer than that of the seabed, the deformations of seabed and breakwater are not compatible at their interface. The relatively large displacements of seabed foundation lead to that there is tensile stress zone at the bottom of breakwater for $\sigma'_x$ and $\sigma'_y$. Furthermore, due to this kind of inconsistent deformation properties between the seabed and breakwater at their interface, there are also two shear stress concentration zones for $\tau_{xy}$ at the bottom of breakwater. As shown in Fig. 7, the direction of $\tau_{xy}$ in the two zones is opposite. The shear stress $\tau_{yz}$ concentrates in the region under the breakwater in lower seabed under the loading of breakwater.

As shown in Fig. 7, the magnitude of $\tau_{xz}$ is much greater than that of $\tau_{xy}$ and $\tau_{yz}$. The concentrated zone of $\tau_{xz}$ locates at the two lateral sloped sides of breakwater, and the zone in seabed foundation near to the toes of the breakwater. The concentration zone of the shear stress ($\tau_{xz}$) in breakwater and seabed would be the potential area where the collapse of breakwater and the shear failure of seabed foundation occur. In Fig. 8, because that the section ($x=277$ m) is near to the symmetric plane $x=276.5$ m, the magnitude of $\tau_{xy}$ and $\tau_{xz}$ is much smaller than that at other sections. Moreover, it is found in Figs. 7 and 8 that the concentration of $\tau_{yz}$ only occurs in the region under breakwater heads.

### 4.2. Soil displacements

Fig. 9 illustrates the distributions of displacements ($u_s$, $v_s$ and $w_s$) in a seabed at sections $y=96$ m and $x=167.5$ m. As shown in the figure, the magnitude of displacements ($u_s$ and $v_s$) is apparently small, which implies that the effect of breakwater is limited at these two sections. The soil displacement ($w_s$) in seabed is layered, indicating that the effect of the rubble mound breakwater on $w_s$ basically disappear because that the two sections are far away the breakwater. However, the seabed subsides under the hydrostatic pressures, and the final settlement of seabed surface is about 62 mm.

Fig. 10 shows the distributions of soil displacements ($u_s$, $v_s$ and $w_s$) in a seabed at sections $y=180$ m and $x=276.5$ m. It is observed from Fig. 10(a) that the construction of rubble mound breakwater on seabed has significant effects on the horizontal displacement of seabed ($u_s$) under hydrostatic pressure loading. The gravity of breakwater makes the seabed move around taking the breakwater as the center in the process of consolidation. Meanwhile, the breakwater compresses the seabed at vertical direction, and subsides downward. The seabed beneath toes of the breakwater could move to the two lateral sides about 10 mm maximally, while the

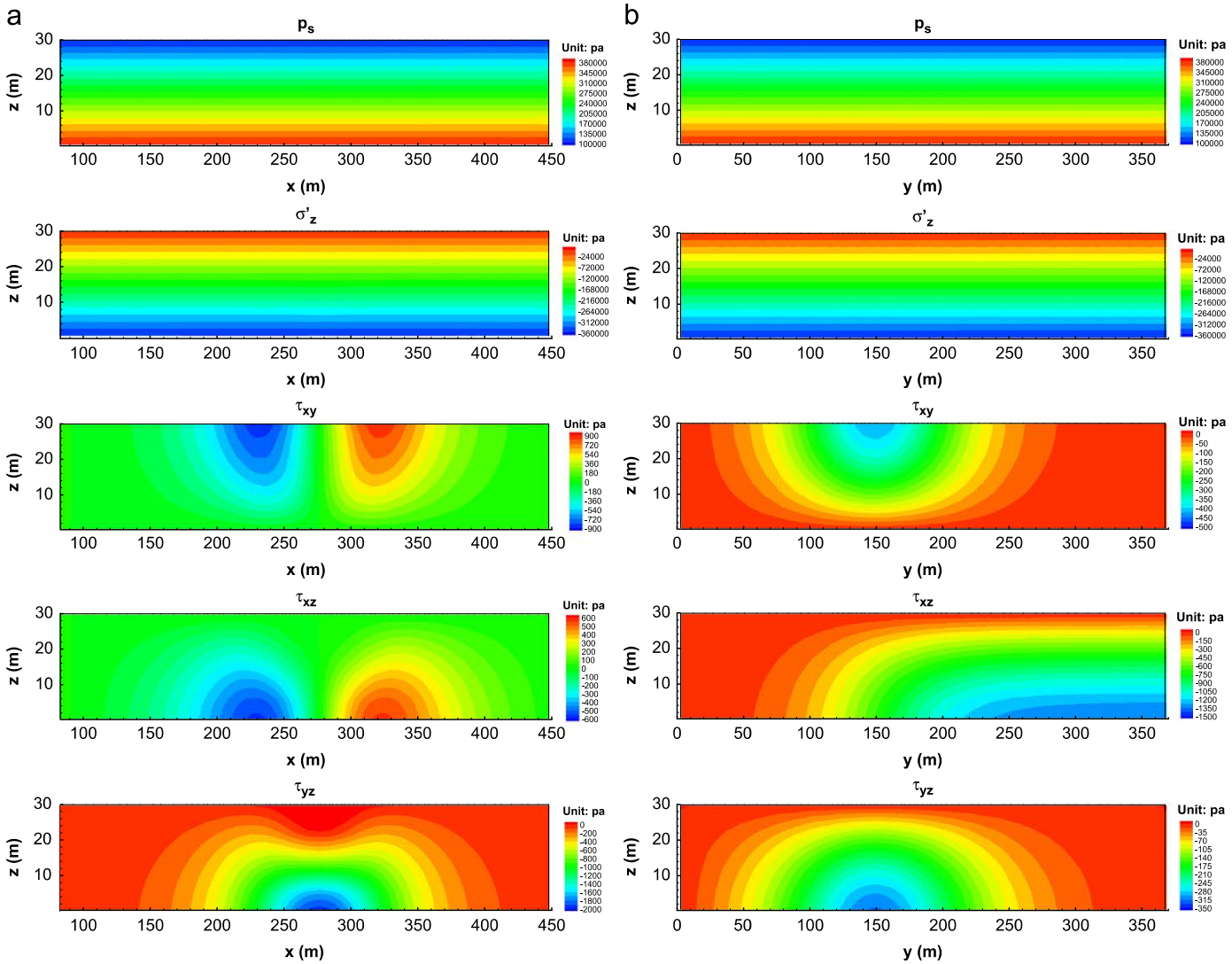


**Fig. 6.** Distributions of pore pressures, effective stresses and shear stresses in seabed at two sections (a) $y$=98.7 m and (b) $x$=167.5 m.

movement of seabed in the $y$-direction maximally is about 8.3 mm. The final settlement of the rubble mound breakwater built on seabed is about 100 mm. From the distribution of $v_s$ at section $x$=276.5 m, it is found that the maximum horizontal displacement ($v_s$) occurs near breakwater heads.

### 4.3. *Effect of rubble mound breakwaters*

The results presented in Figs. 6–10 only provide the overall effects of the breakwater on the consolidation of seabed. In this section, the effects of a breakwater on the stresses and displacements in a seabed are investigated quantitatively.

The distributions of stresses along three typical lines parallel to the $y$-axis are presented in Fig. 11. They are: ($y$, $z$)=(74, 25.2), far away from the breakwater (dotted line); ($y$, $z$)=(151, 25.2), at the breakwater head (blue line); and ($y$, $z$)=(227, 25.2), beneath the breakwater (red line) respectively. In the region far away from the breakwater, the shear stresses are zeros and the effective normal stresses come from the self-gravity of seabed soil. As shown in the figure, $\sigma'_x$ and $\sigma'_y$ are about 30 kPa, and $\sigma'_z$ is about 60 kPa. However, in the region beneath the breakwater or at the breakwater head, the gravity of breakwater makes the effective stresses $\sigma'_x$, $\sigma'_y$ and $\sigma'_z$ increase significantly. Among these, $\sigma'_x$, $\sigma'_y$ and $\sigma'_z$ reach up to about 50 kPa, 55–70 kPa and 170 kPa, respectively at depth of 4.8 m below the seabed surface ($z$=25.2 m). The shear stresses, especially the $\tau_{xz}$, will also increase in the region. The dramatical change of $\tau_{xz}$ in the region near to the toe of breakwater would cause the shear failure of seabed foundation.

Figs. 12 and 13 further present the distributions of stresses on three typical lines which are parallel to the $x$- and $z$-axis, respectively. Similar conclusions can be draw from these figures, as that in Fig. 11. However, a sharp increase of effective normal stresses ($\sigma'_x$, $\sigma'_y$ and $\sigma'_z$) at breakwater head is observed in Fig. 12. It is observed that $\tau_{xz}$ along the line ($x$, $z$)=(277, 25.2 m) is nearly zero. This is because that the line is closed to the symmetrical plane $x$=276.5 m. On the symmetrical plane $x$=276.5 m, the $\tau_{xz}$ is 0. In fact, the magnitude of $\tau_{xz}$ at other place deviating the symmetrical plane could reach up to 30–40 kPa, which may have potential to cause shear failure of seabed foundation. As shown in Fig. 13, the magnitude of $\tau_{xy}$ and $\tau_{yz}$ is small relative to $\tau_{xz}$ at toes of a breakwater.

Fig. 14 demonstrates the distributions of displacements along nine typical lines in seabed (classified into three groups). Each group (containing three lines) is parallel with $x$, $y$ or $z$ axis. As shown in the figure, the following points are observed:

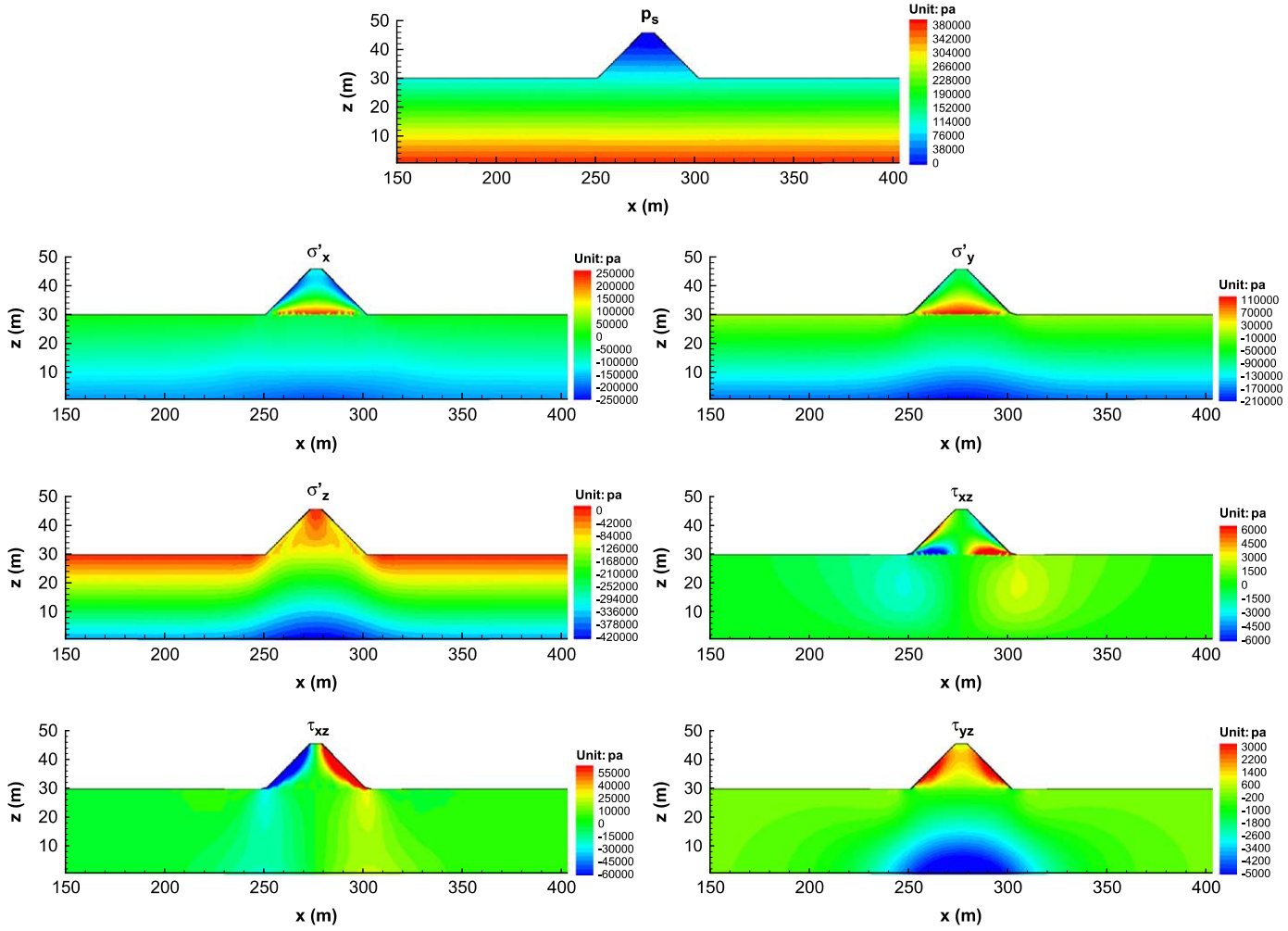


**Fig. 7.** Distributions of pore pressures, effective stresses in seabed at section $y=181.1$ m.

(1) Under the gravity of breakwater and hydrostatic pressure loading, the seabed is compressed and moves toward around and the breakwater subsides vertically.
(2) Due to that the horizontal displacement $u_s$ at $+x$ and $-x$ direction is symmetric, the displacement $u_s$ on the symmetric plane ($x=276.5$ m) is zero.
(3) In the region near breakwater heads, the displacement $v_s$ is obviously greater than that in other soil displacements in seabed. This is the reason why the concentration of the shear stress ($\tau_{xy}$ and $\tau_{yz}$) occurs near the head of breakwater.
(4) In the region far away from the breakwater, the deformation of seabed basically is not affected by the breakwater. The settlement of seabed under hydrostatic pressure and self-weight is about 62 mm. In the region near to or under the breakwater, the compression settlement in seabed increase significantly. The maximum settlement in the seabed reach up to 100 mm.
(5) Based on the distributions of $w_s$ (as shown in Fig. 14(a)), it is found that the vertical displacements ($w_s$) near to the toes of breakwater are less than 60 mm, which is the same as the case far away the breakwater. This phenomenon would be attributed to the fact that the breakwater compresses the seabed and makes the seabed move toward two lateral sides ($+x$ and $-x$ direction). Then, the shear stress $\tau_{xz}$ with large magnitude is generated in the region beneath and near to breakwater heads. Under the applying of $\tau_{xz}$, the seabed foundation near to the toes of breakwater uplifts. If the uplift displacements of seabed foundation reach up to a critical value, the shear failure will occur.

### 4.4. Parametric study

Numerous parameters are involved in the determination of the final consolidation status of a porous seabed under the hydrostatic pressure and the gravity of rubble mound breakwater. These include Young's modulus ($E$), permeability ($k$) and the degree of saturation ($S_r$), and the water depth ($d$). However, how these parameters affect the consolidation of seabed has not been fully understood. In the section, a parametric study is conducted to demonstrate the effect of seabed parameters ($E$, $k$, $S_r$) and water depth ($d$) on the consolidation status of seabed.

In practical engineering, the major concerns of coastal engineers in the design of a breakwater are: (1) the final settlement of the designed breakwater on seabed after consolidation; (2) whether instability of the seabed foundation under or near to the toes of designed breakwater would occur. Excessive settlement of breakwater, and shear failure of seabed foundation are two key factors for the analysis of instability of rubble mound breakwater. In this study, the final settlement of breakwater on seabed ($w_s$) and the shear stress ($\tau_{xz}$) at point ($x$, $y$, $z$)=(248.6, 202.7, 29.25) are chosen as the representative quantities to examine the effect of the aforementioned parameters ($E$, $k$, $S_r$ and $d$) on the seabed consolidation under hydrostatic pressure

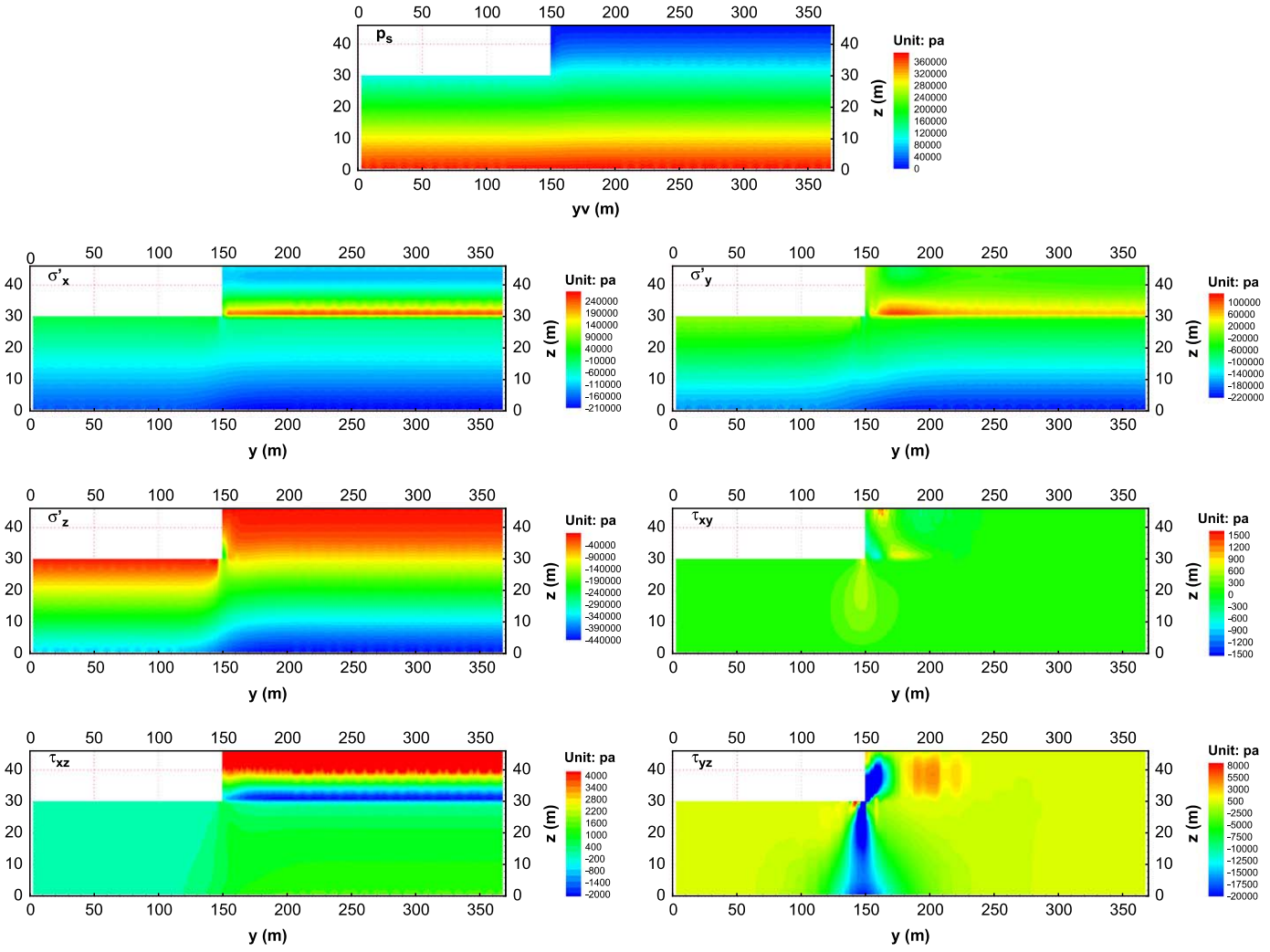


**Fig. 8.** Distributions of pore pressures, effective stresses in seabed at section $x=277$ m.

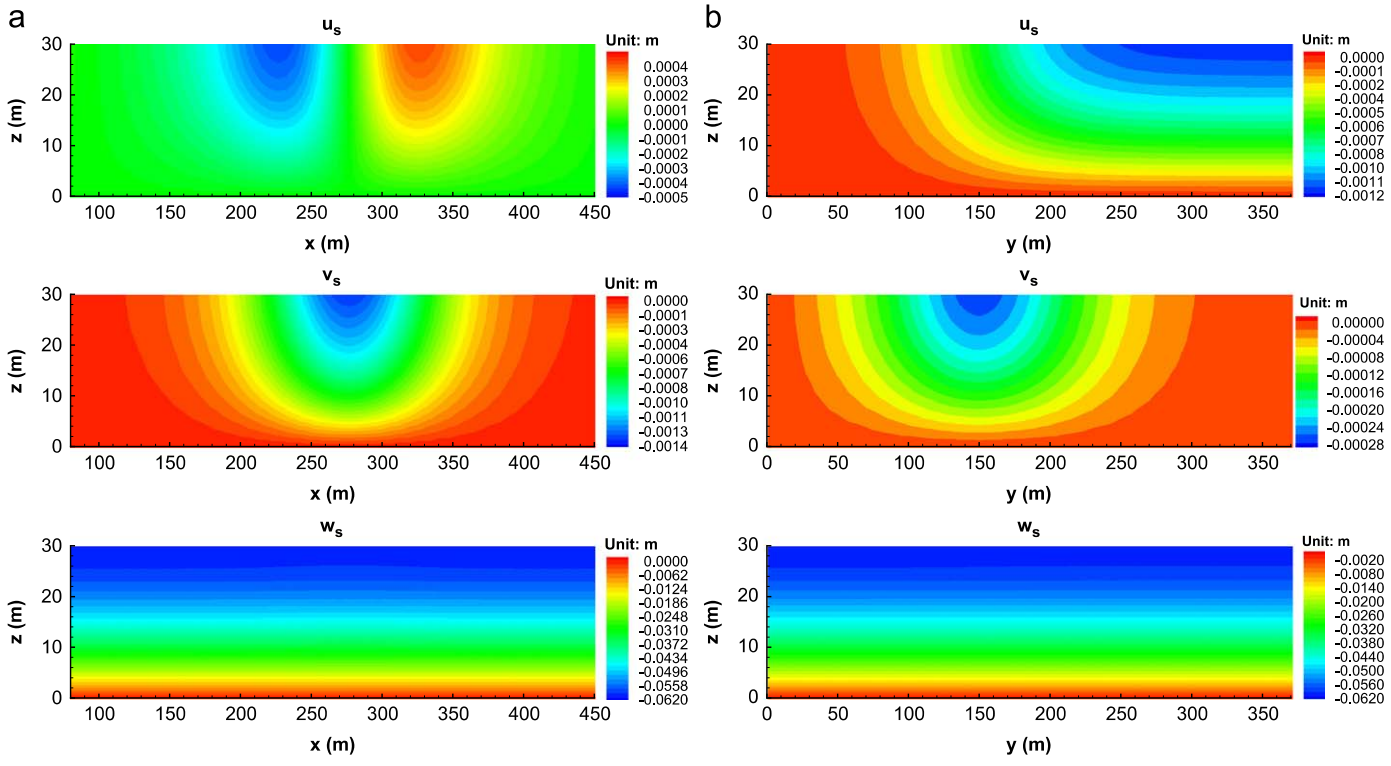


**Fig. 9.** Distributions of displacements in seabed at sections (a) $y=96$ m and (b) $x=167.5$ m.

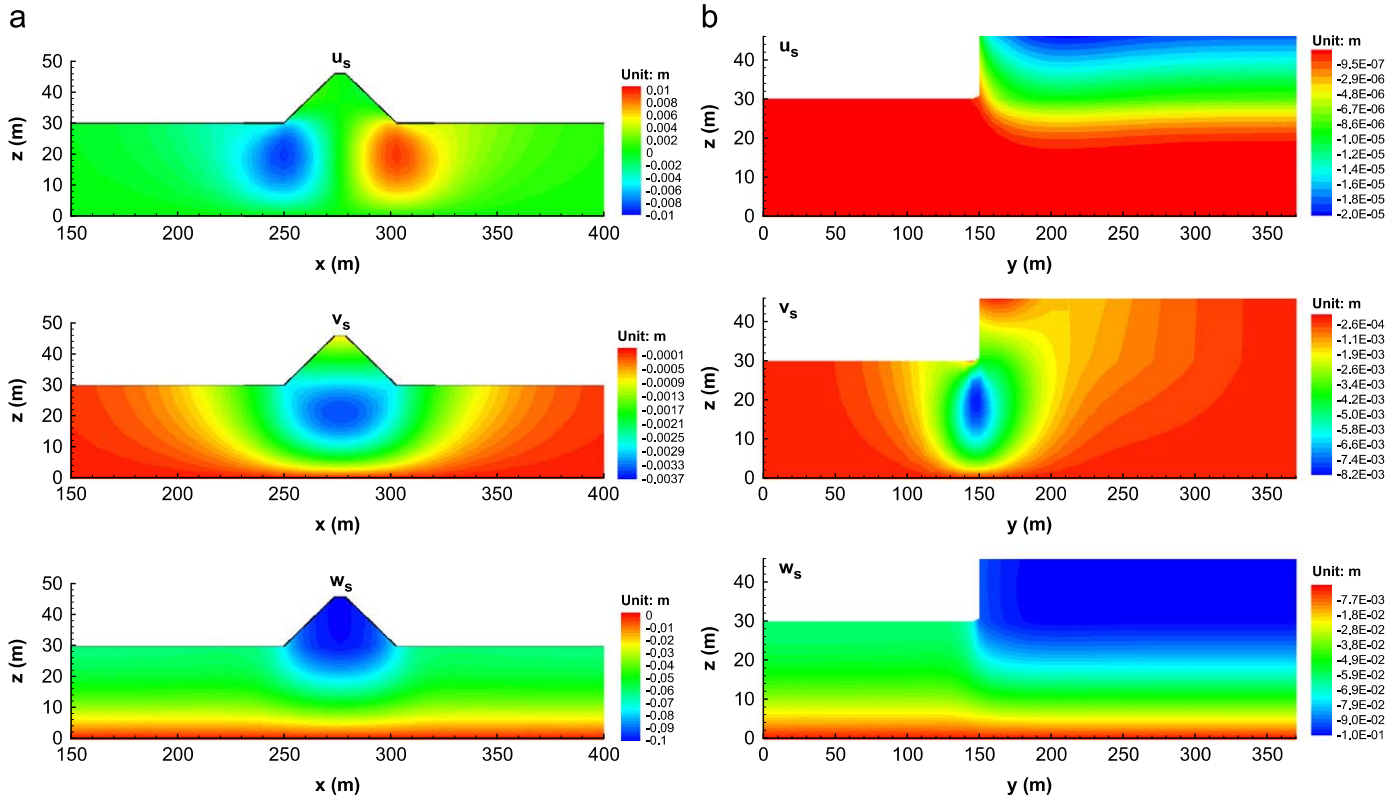


**Fig. 10.** Distributions of displacements in seabed at sections (a) $y=180$ m and (b) $x=276.5$ m.

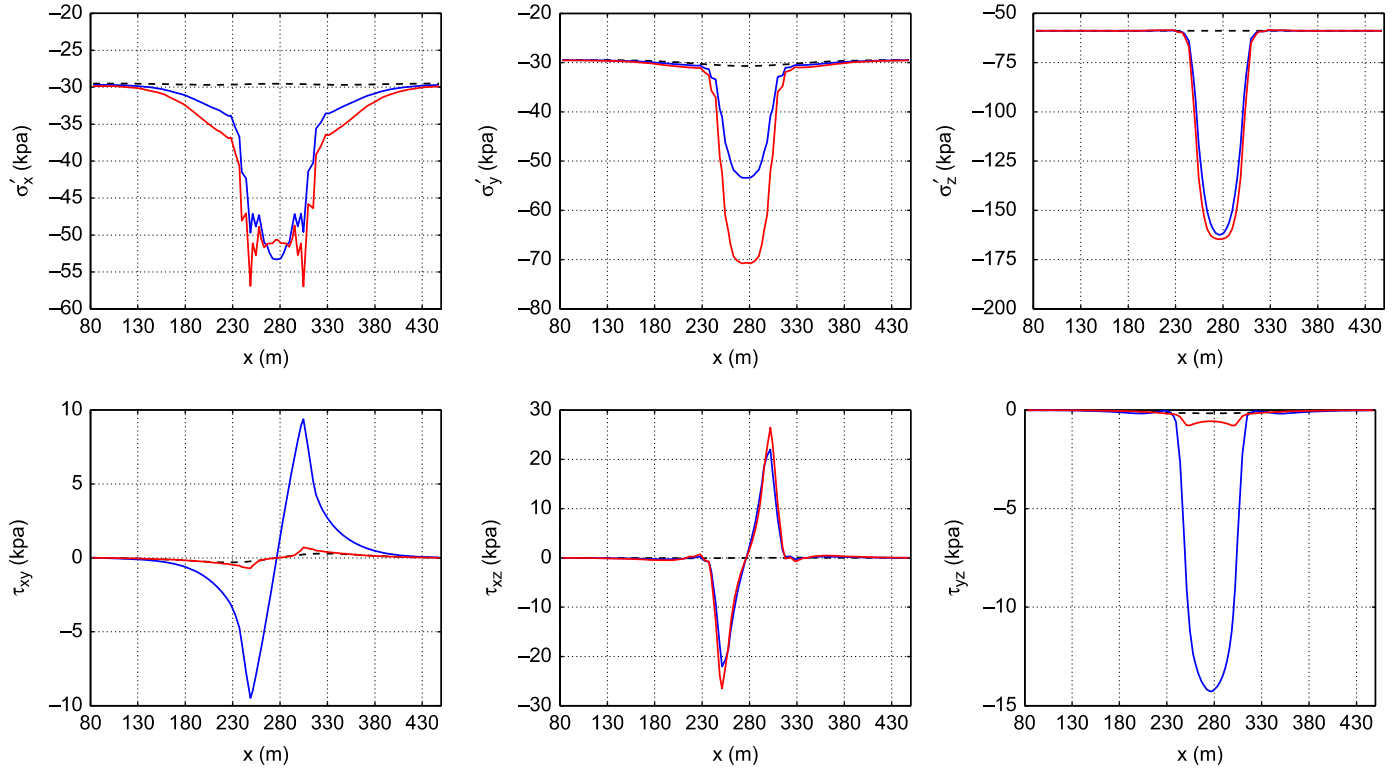


**Fig. 11.** Distributions of stresses on three typical lines which are parallel with the $y$-axis: dashed line: ($y$, $z$)=(74, 25.2) far away from the breakwater, blue line: ($y$, $z$)=(151, 25.2) at the breakwater head; and red line: ($y$, $z$)=(227, 25.2) beneath the breakwater. (For interpretation of the references to color in this figure caption, the reader is referred to the web version of this article.)

and rubble mound breakwater. The representative parameters are: $E=6.0\times10^7$ N/m$^2$, $k=1.0\times10^{-4}$ m/s, $S_r=98\%$ and $d=10$ m, while parameters vary one by one.

As shown in Table 3, the Young's modulus $E$ is the most sensitive parameter to affect the seabed consolidation status. The stiffer the seabed foundation, the smaller the settlement of the

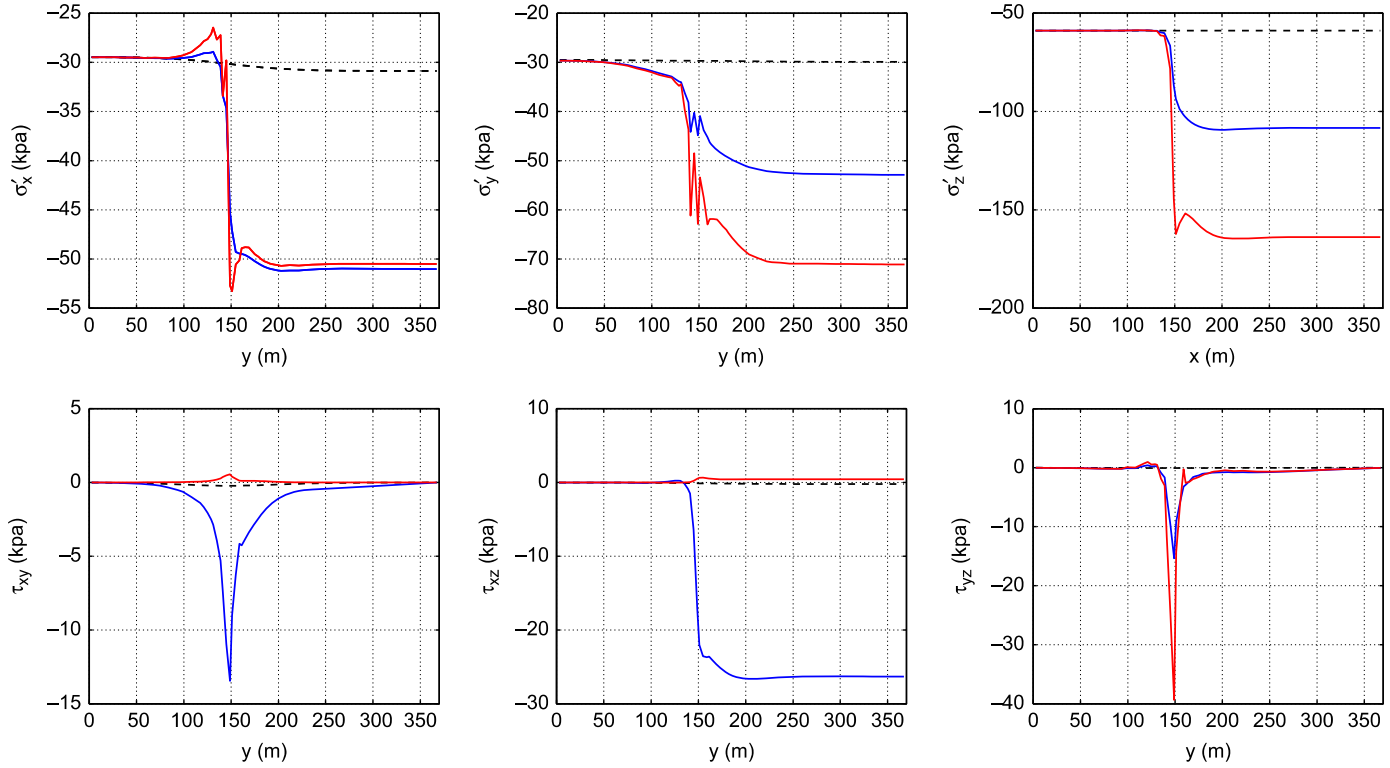


**Fig. 12.** Distributions of pore pressure, stresses on three typical lines parallel to the *x*-axis: dashed line: $(x, z)=(167.5, 25.2)$ far away from the breakwater, blue line: $(x, z)=(250, 25.2)$ at the breakwater head; red line: $(x, z)=(277, 25.2)$ beneath the breakwater. (For interpretation of the references to color in this figure caption, the reader is referred to the web version of this article.)

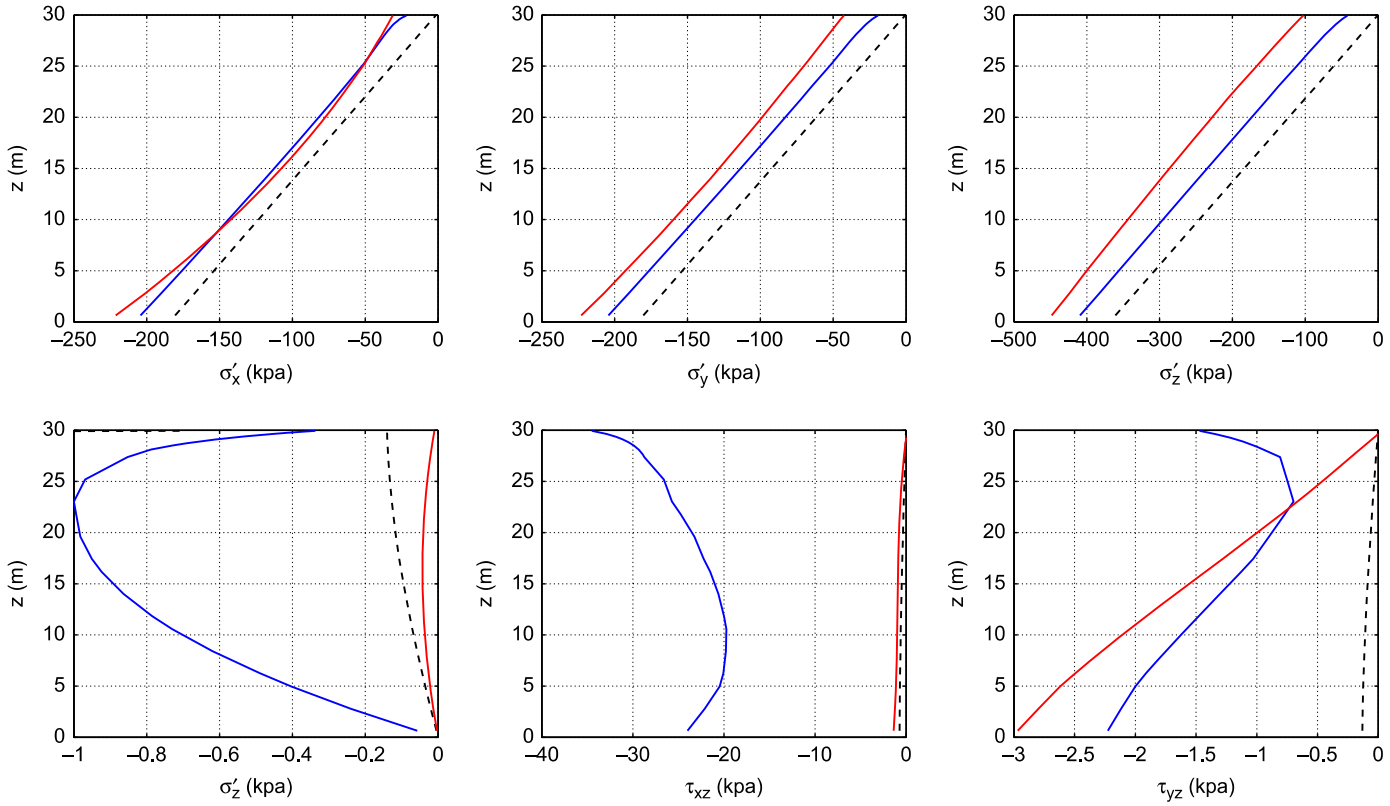


**Fig. 13.** Distributions of pore pressure, stresses on three typical lines which are parallel with the *z*-axis: dashed line: $(x, z)=(167.5, 224)$ far away from the breakwater; blue line: $(x, z)=(250, 224)$ at the breakwater head, red line: $(x, z)=(277, 224)$ beneath the breakwater. (For interpretation of the references to color in this figure caption, the reader is referred to the web version of this article.)

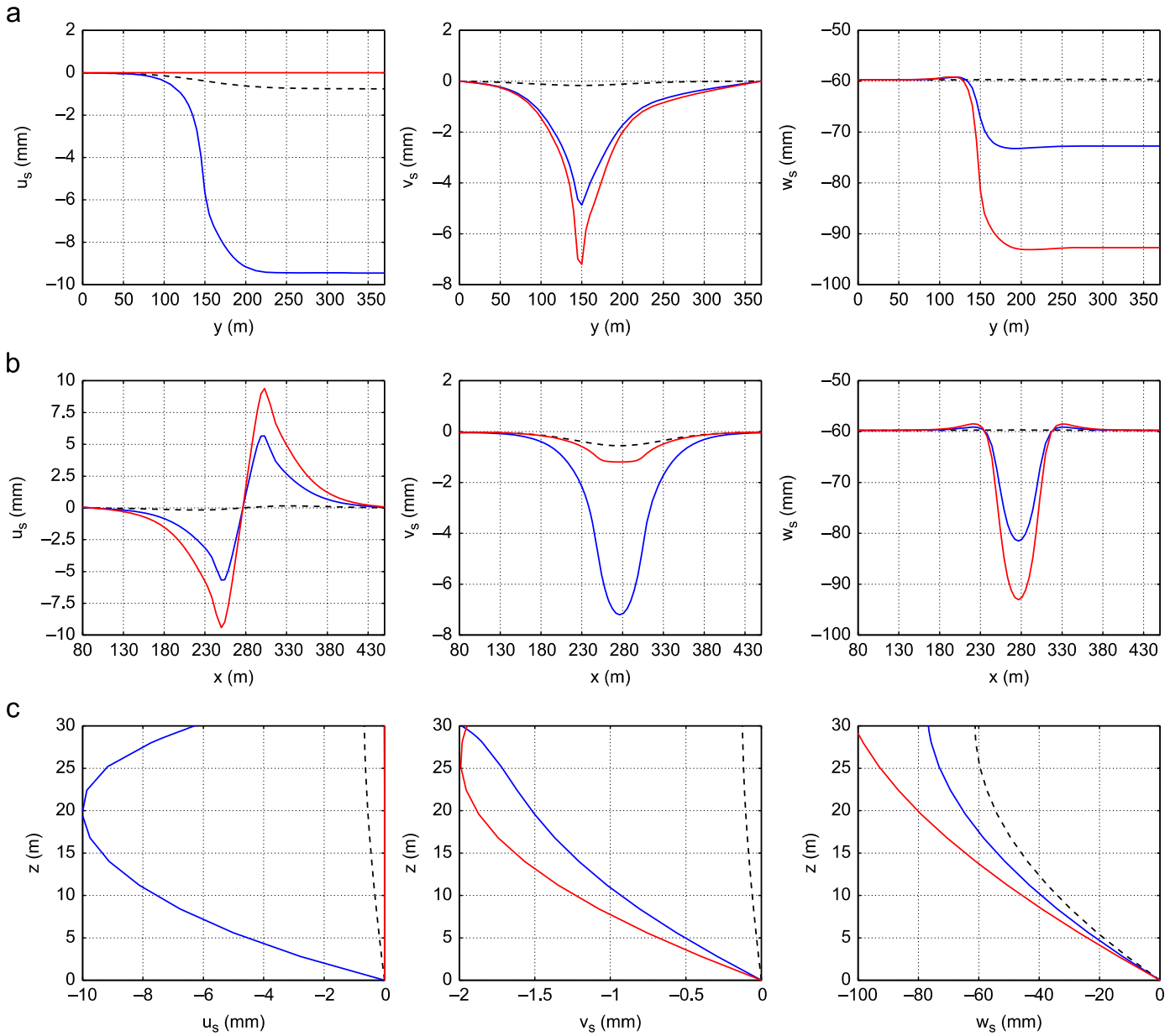


**Fig. 14.** Distributions of displacements on nine typical lines parallel with the $x$, $y$ and $z$-axis respectively. (a) Parallel to $x$-axis. Dotted line: $(y, z)=(72, 25.2)$; blue line: $(y, z)=(155, 25.2)$; red line: $(y, z)=(224, 25.2)$. (b) Parallel to $y$-axis. Dotted line: $(x, z)=(155, 25.2)$; blue line: $(x, z)=(250, 25.2)$; red line: $(x, z)=(276.5, 25.2)$. (c) Parallel to $z$ axis. Dotted line: $(x, y)=(155, 200)$; blue line: $(x, y)=(250, 200)$; red line: $(x, y)=(276.5, 200)$. (For interpretation of the references to color in this figure caption, the reader is referred to the web version of this article.)

**Table 3**
The settlement of breakwater and the shear stress $\tau_{xz}$ at (248.6 m, 202.7 m, 29.25 m) which is near to the foot of breakwater in parametric study.

| Variable | Results | | Variable | Results | | Item | Results | | Item | Results | |
|---|---|---|---|---|---|---|---|---|---|---|---|
| $E$ (Mpa) | $w_s$ (mm) | $\tau_{xz}$ (kPa) | $k$ (m/s) | $w_s$ (mm) | $\tau_{xz}$ (kPa) | $S_r$ (%) | $w_s$ (mm) | $\tau_{xz}$ (kPa) | $d$ (m) | $w_s$ (mm) | $\tau_{xz}$ (kPa) |
| 30.0 | 181.84 | −27.55 | $10^{-6}$ | 93.41 | −21.79 | 95 | 93.34 | −21.77 | 5 | 99.87 | −21.37 |
| 60.0 | 93.36 | −21.77 | $10^{-4}$ | 93.36 | −21.77 | 98 | 93.36 | −21.77 | 10 | 93.36 | −21.77 |
| 100.0 | 57.17 | −18.04 | $10^{-2}$ | 93.43 | −21.81 | 100 | 93.42 | −21.77 | 20 | 88.52 | −20.84 |

breakwater, and the magnitude of shear stress $\tau_{xz}$ in the region near to the toes of the breakwater. Therefore, it is improved that the hard seabed is benefit for the stability of marine structures. It is also observed that other parameters ($k$ and $S_r$) only has little effect on the final settlement of breakwater and the $\tau_{xz}$ developed in the seabed foundation. However, the influence of water depth ($d$) on the final settlement is visible. Based on the parametric study, it is concluded that the stiffness and bearing capacity of seabed foundation should be the primary factors considered in design of a breakwater.

## 5. Conclusions

The main objective of this study is to investigate the consolidation process of seabed foundation under hydrostatic water pressures and rubble mound breakwaters. A three-dimensional finite element model, based on Biot's poro-elastic theory, is adopted. Based on numerical examples presented, the following conclusions can be drawn.

(1) The breakwater basically does not affect the effective stresses $\sigma'_x$, $\sigma'_y$ and $\sigma'_z$ in the region far away the breakwater. However, in the same region, the effect on the shear stress $\tau_{xy}$, $\tau_{yz}$ and $\tau_{xz}$ can be observed, even though it is insignificant.
(2) In the region near to or under the rubble mound breakwater, the effect of breakwater on the stress fields is significant. The effective stresses $\sigma'_x$, $\sigma'_y$ and $\sigma'_z$ and shear stresses $\tau_{xy}$, $\tau_{yz}$ and $\tau_{xz}$ increase dramatically. Furthermore, the $\tau_{xy}$ and $\tau_{xz}$ concentrate in the zone under the toes of the breakwater. This could be the reason that the shear failure frequently occurs in seabed foundation under the breakwater. Once the shear failure occurring, the seabed soil near to the toes of breakwater will uplift significantly.
(3) Under the gravity of breakwater loading, the seabed soil moves toward around; and the breakwater compresses the seabed foundation, and subsides. The final settlement is about 100 mm. In the region far away the breakwater, the seabed also subsides itself under the hydrostatic pressure and self-weight. The final settlement of seabed surface is about 62 mm. It is noted that the final settlement of breakwater and seabed are mainly dependent on the Young's modulus $E$ of seabed soil.
(4) The parametric study indicates that the Young's modulus $E$ significantly affects the seabed consolidation status. The hard seabed could effectively decrease the settlement of breakwater, and the magnitude of shear stress $\tau_{xz}$ in the region near to the foots of breakwater.

In this paper, the present model was only verified with one-dimensional Terzagh's consolidation theory, because there is no laboratory experimental data and field measurements available in the literature. It will be worthwhile to conduct a series of experiments for the pore pressure and settlements under consolidation process before wave loading in the future study.

## Acknowledgements

The authors are grateful for the financial support from EPSRC #EP/G006482/1 and Sichuan University State Key Laboratory of Hydraulics and Mountain River Engineering Open Fund Scheme #SKLH-OF-1005 (China), and National Foundation Council (NSFC) Grant #41176073 (China).

## References

Biot, M.A., 1941. General theory of three-dimensional consolidation. J. Appl. Phys. 26 (2), 155–164.
Booker, J.R., 1973. A numerical method for the solution of Biot's consolidation theory. Q. J. Mech. Appl. Math. 26 (4), 457–470.
Cavalcanti, M.C., Telles, J.C.F., 2003. Biot's consolidation theory—application of BEM with time independent fundamental solutions for poro-elastic saturated media. Eng. Anal. Boundary Elem. 27 (2), 145–157.
Chung, S.G., Kim, S.K., Kang, Y.J., Im, J.C., Prasad, K.N., 2006. Failure of a breakwater founded on a thick normally consolidated clay layer. Géotechnique 56 (3), 393–409.
Ferronato, M., Castelletto, N., Gambolati, G., 2010. A fully coupled 3-d mixed finite element model of biot consolidation. J. Comput. Phys. 229 (12), 4813–4830.
Franco, L., 1994. Vertical breakwaters: the Italian experience. Coastal Eng. 22 (1–2), 31–55.
Hua, L., 2011. Stable element-free Galerkin solution procedures for the coupled soil–pore fluid problem. Int. J. Numer. Methods Eng. 86 (8), 1000–1026.
Jeng, D.-S., Cha, D.H., Lin, Y.S., Hu, P.S., 2001. Wave-induced pore pressure around a composite breakwater. Ocean Eng. 28 (10), 1413–1432.
Jeng, D.-S., Ou, J., 2010. 3-d models for wave-induced pore pressure near breakwater heads. Acta Mech. 215, 85–104.
Kelln, C., Sharma, J., Hughes, D., Graham, J., 2009. Finite element analysis of an embankment on a soft estuarine deposit using an elastic viscoplastic soil model. Can. Geotech. J. 46 (3), 357–368.
Korsawe, J., Starke, G., Wang, W., Kolditz, O., 2006. Finite element analysis of poro-elastic consolidation in porous media: standard and mixed approaches. Comput. Methods Appl. Mech. Eng. 195 (9–12), 1096–1115.
Lundgren, H., Lindhardt, J.H.C., Romold, C.J., 1989. Stability of breakwaters on porous foundation. In: Proceeding of 12th International Conference on Soil Mechanics and Foundation Engineering, vol. 1, pp. 451–454.
Mase, H., Sakai, T., Sakamoto, M., 1994. Wave-induced pore water pressure and effective stresses around breakwater. Ocean Eng. 21 (4), 361–379.
Miga, M.I., Paulsen, K.D., Kennedy, F.E., 1998. Von Neumann stability analysis of Biot's general two-dimensional theory of consolidation. Int. J. Numer. Methods Eng. 43 (5), 955–974.
Mizutani, N., Mostarfa, A., Iwata, K., 1998. Nonlinear regular wave, submerged breakwater and seabed dynamic interaction. Coastal Eng. 33, 177–202.
Mostafa, A.M., Mizutani, N., Iwata, K., 1999. Nonlinear wave, composite breakwater and seabed dynamic interaction. J. Waterw. Port Coastal Ocean Eng. ASCE 125 (2), 88–97.
Sloan, S.W., Abbo, A.J., 1999. Biot consolidation analysis with automatic time stepping and error control part 1: theory and implementation. Int. J. Numer. Anal. Methods Geomech. 23 (6), 467–492.
Terzaghi, K., 1925. Erdbaumechanik auf Bodenphysikalischer Grundlage. F. Deuticke, Vienna, Deuticke.
Ulker, M., Rahman, M.S., Guddati, M.N., 2010. Wave-induced dynamic response and instability of seabed around caisson breakwater. Ocean Eng. 37, 1522–1545.
Wang, H.F., 2000. Theory of Linear Poroelasticity with Application to Geomechanics and Hydrogeology. Princeton University Press, Princeton, NJ.
Wang, J.G., Karim, M.R., Lin, P.Z., 2007. Analysis of seabed instability using element free Galerkin method. Ocean Eng. 34 (2), 247–260.
Wang, J.G., Xie, H., Leung, C.F., 2009. A local boundary integral-based meshless method for Biot's consolidation problem. Eng. Anal. Boundary Elem. 33 (1), 35–42.
Wang, J.G., Zhang, B., Nogami, T., 2004. Wave-induced seabed response analysis by radial point interpolation meshless method. Ocean Eng. 31 (1), 21–42.
Yin, J.-H., Zhu, J.-G., 1999. Elastic viscoplastic consolidation modelling and interpretation of pore-water pressure responses in clay underneath Tarsiut Island. Can. Geotech. J. 36 (4), 708–717.
Zhang, J.-S., Jeng, D.-S., Liu, P.L.-F., 2011. Numerical study for waves propagating over a porous seabed around a submerged permeable breakwater PORO-WSSI II model. Ocean Eng. 38 (7), 954–966.
Zienkiewicz, O.C., Chang, C.T., Bettess, P., 1980. Drained, undrained, consolidating and dynamic behaviour assumptions in soils. Géotechnique 30 (4), 385–395.